Physica D 444 (2023) 133595

Contents lists available at ScienceDirect

Physica D

journal homepage: www.elsevier.com/locate/physd

The two-process model for sleep–wake regulation: A nonsmooth dynamics perspective

Mustafa Şaylı [a,1], Anne C. Skeldon [b,c,1], Rüdiger Thul [a,1], Rachel Nicks [a,1], Stephen Coombes [a,*,1]

[a] Centre for Mathematical Medicine and Biology, School of Mathematical Sciences, University of Nottingham, Nottingham, NG7 2RD, UK
[b] Department of Mathematics, Faculty of Electronics and Physical Sciences, University of Surrey, Guildford GU2 7XH, UK
[c] UK Dementia Research Institute, Care Research and Technology Centre at Imperial College, London and the University of Surrey, Guildford, UK

ARTICLE INFO

Article history:
Received 30 May 2022
Received in revised form 10 October 2022
Accepted 14 November 2022
Available online 26 November 2022
Communicated by Dmitry Pelinovsky

Keywords:
Two process model
Sleep regulation
Nonsmooth dynamics
Saltation operator
Lyapunov exponent
Arnol'd tongue

ABSTRACT

Since its inception four decades ago the two-process model introduced by Borbély has provided the conceptual framework to explain sleep–wake regulation across many species, including humans. At its core, high level notions of circadian and homeostatic processes are modelled with a low dimensional description in the form of a one dimensional nonautonomous and nonsmooth flow, with the rate of change of homeostatic sleep pressure switching at specific times. These *events* in time can be described by an implicit map from one switching time to another and have given rise to an elegant mathematical description of periodic orbits and their instabilities using the theory of iterated maps. In this paper we show that an equivalent description can be obtained from a direct analysis of the underlying nonsmooth flow. We further show how to construct the Lyapunov exponent of the nonsmooth flow and use this to uncover a more detailed picture of the Arnol'd tongue structure of the model.

Given the growing interest in studying networks of sleepers, where interactions may occur continuously throughout the day–night cycle and not just at event times, we advocate for the future use of techniques from nonsmooth dynamical systems in studying networks of the two-process model.

1. Introduction

Sleep is necessary for humans to maintain a healthy mind and functioning body. Sleep aids the development of the immune system, [1] and is crucial for learning and memory [2]. Sleep resets the pain perception system [3]. Poor or mistimed sleep is associated with many health problems [4], including psychotic disorders and depression [5], and increased risk of diabetes [6], obesity [7], and cardiovascular disease [8]. The strong association between sleep and health necessitates a good understanding of sleep–wake regulation processes.

Mathematical models have been used as a powerful instrument to explore biological mechanisms of sleep–wake regulation for many years, for early models see Moore-Ede et al. [9]. Most classical models have at least two oscillators capturing the need for sleep after being awake for a period of time and the approximately daily (circadian) rhythm of the so-called master clock in the suprachiasmatic nucleus of the brain [10–12]. Others consider the cyclic transitions between rapid eye movement and nonrapid eye movement sleep which, in humans, have an approximately 90 min period and are therefore an example of ultradian rhythms [13,14]. More recent models have developed a more 'physiological' approach proposing neuronal models that model sleep–wake regulation through the interaction of a small number of interacting populations of neurons [15,16]. However, the two-process model captures many essential features of the dynamics of these more complex models [17,18] and therefore remains relevant [19].

The two-process model itself has had a major impact on the field of sleep research, with over 4,500 citations at the time of writing and providing the conceptual framework and a mechanistic understanding for many laboratory and field studies. The model has two interacting oscillators: a circadian oscillator (sleep independent process) and a homeostatic oscillator (sleep dependent process). The homeostatic sleep process represents a regulatory process aimed at keeping physiological sleep need within reasonable bounds. The homeostatic process is modelled by a sleep pressure that increases monotonically during wake and decreases monotonically during sleep. Switching from wake to sleep and from sleep to wake occurs at upper and lower thresholds respectively. The thresholds are modulated by a periodic function representing the circadian oscillation, see Fig. 1. Nakao

* Corresponding author.
E-mail address: stephen.coombes@nottingham.ac.uk (S. Coombes).
[1] All authors contributed equally to this paper.

https://doi.org/10.1016/j.physd.2022.133595

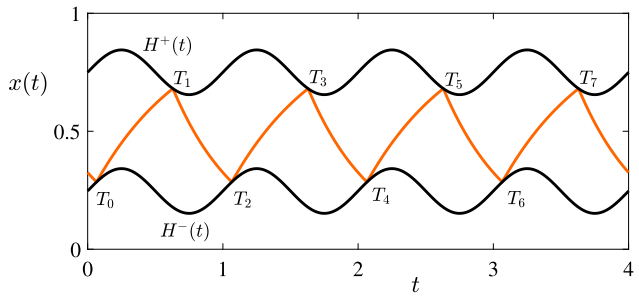

Fig. 1. A (1, 1) periodic orbit (one sleep–wake episode in one day) of the two-process model with $C(t) = \sin(2\pi t)$. The homeostatic sleep pressure (shown in light brown) increases during wake and decreases during sleep. The upper and lower thresholds are shown in black. Switching from wake (sleep) to sleep (wake) takes place at the upper (lower) threshold crossing. Parameters: $\tau_w = 0.70$, $\tau_s = 0.5$, $H_0^+ = 0.75$, $H_0^- = 0.2469$, $a^\pm = 0.09478$.

et al. [20,21] have described these switching *events* using a one-dimensional map with a *gap* [22–24] (and linked this to a circle map using periodicity of the circadian activity).

As first observed in [11], the two-process model exhibits a wide range of different sleep patterns including those representing a single sleep–wake episode in a day, (monophasic sleep, characteristic of adult humans) and those with many sleep episodes a day, (polyphasic sleep, characteristic of human babies and small mammals). Using the circle map framework, Bailey et al. performed a detailed analysis to understand the types of bifurcation that occur in the two-process model and the underlying bifurcation structure that gives regions of existence of different stable solutions representing different numbers of sleep episodes a day [25].

Given the success of the two-process model at the level of a single sleeper it is natural to use it as a starting point for network studies relevant for understanding the behaviour of adolescent social groups where sleep timing may be dictated by social media interactions and for sleep–wake patterns of cohabiting partners. Indeed, given the human social prevalence for couple bed sharing [26], it is somewhat surprising that there is very little modelling work in this latter context. However, since sleeper–sleeper interactions may be continuous in time the discrete map based approach for analysing the two-process model does not lend itself well to such network studies. There is therefore a need to develop analytical tools that are better able to capture continuous interactions. We also note that there is an increased recognition that sleep homeostasis and circadian rhythmicity may not be so neatly separated into two distinct processes, and that sleep homeostasis may depend on circadian phase and vice versa [27]. Hence in future generations of models of sleep regulation, a nonsmooth flow approach may be more appropriate.

We note that for the original two-process model, the nonsmooth flow perspective is complementary to the map-based perspective. The map-based approach makes explicit the connection between the two-process model and other oscillatory systems and leads naturally to understanding how the dynamics are organised in terms of an Arnol'd tongue framework. However computations, and relating features in the maps to model behaviour (e.g., the creation of gaps), requires consideration of the nonsmooth flow.

In this paper, we therefore develop a nonsmooth flow perspective that continuously captures homeostatic and circadian interactions. Since an essential first step in developing a new analytical approach is that it should recover previous results, our focus here is on a single sleeper. Throughout we therefore compare our nonsmooth approach with the map-based approach.

In Section 2 we introduce the two-process model and its representation as a piecewise linear ordinary differential equation system with switches, namely a type of nonsmooth flow. The construction of continuous time periodic orbits is considered in Section 3 where, with the use of *saltation* operators we show how to augment standard Floquet theory to determine the stability of periodic solutions. The equivalence to the map-based approach for determining solution stability is demonstrated. In Section 4, we show how to determine the Lyapunov exponent for the nonsmooth flow, and subsequently, in Section 5 make use of this to probe some of the details of the Arnol'd tongue structure for the two-process model. Finally, in Section 6 we discuss the natural extensions of the work in this paper to the network level.

2. The two-process model

The two-process model is a fascinating and ostensibly simple piecewise linear model which belongs to a wider class of "threshold" systems, see [24]. The two-process model characterises the timing and distribution of sleep and wake as the interaction of circadian and homeostatic process evolution. The combination of these two oscillatory processes as continuous flows may be formulated as $x = x(t)$, $\dot{x} = \mathrm{d}x/\mathrm{d}t$ and:

$$\dot{x} = \begin{cases} -\dfrac{x}{\tau_w} + \dfrac{1}{\tau_w} & \dot{x} > 0 \text{ and } x(t) < H^+(t) \text{ (wake)} \\ -\dfrac{x}{\tau_s} & \dot{x} < 0 \text{ and } x(t) > H^-(t) \text{ (sleep)}, \end{cases} \tag{1}$$

where

$$H^\pm(t) = H_0^\pm + a^\pm C(t). \tag{2}$$

Here, x represents the homeostatic sleep pressure and $C(t)$ represents the circadian process. Switching from wake to sleep occurs when $\dot{x} > 0$ and $x(t) = H^+(t)$. Switching from sleep to wake occurs when $\dot{x} < 0$ and $x(t) = H^-(t)$.

The model contains six parameters. The parameters τ_s and τ_w are time constants which determine the rate of change of homeostatic sleep pressure during sleep and wake, respectively. Originally, Borbély et al. [28,29] envisaged that the time constants represented the decay of so-called 'slow wave activity', derived from electroencephalogram measurements, and values were extracted from data. The thresholds were phenomenological and a scaling chosen such that homeostatic sleep pressure asymptotes to one during wake and to zero during sleep. The mean values of the thresholds, H_0^+ and H_0^- and the shape of the periodic circadian function $C(t)$ and its amplitude $a^\pm$ were chosen to match experimental data. The circadian function $C(t)$ represents the daily variation in wake propensity and was chosen so that the model replicates the observed functional relationship between sleep duration and sleep onset time. In the simplest case, $C(t)$ is often chosen to have a sinusoidal form, though more complicated forms that include higher harmonics have also been used [29]. Throughout this paper we will choose $C(t)$ to be one of $\sin(2\pi t)$ or $\cos(2\pi t)$. Here, time is scaled so that solutions with period one corresponds to solutions which have a period of one day. (See [30] for further discussion on physiological relevance, restrictions and derivation of the model parameters).

We define $x_w(t, t_0^w)$ as the homeostatic sleep pressure during wake, which starts at $t = t_0^w$ on the lower threshold with the initial value $x_w(t_0^w)$, and $x_s(t, t_0^s)$ as the homeostatic sleep pressure during sleep, which starts at $t = t_0^s$ on the upper threshold with the initial value $x_s(t_0^s)$. Then, from Eqs. (1), the explicit solutions for $x_w(t, t_0^w)$ and $x_s(t, t_0^s)$ are

$$x_w(t, t_0^w) = 1 - [1 - x_w(t_0^w)]\mathrm{e}^{-\frac{t - t_0^w}{\tau_w}}, \tag{3}$$

$$x_s(t, t_0^s) = x_s(t_0^s)\mathrm{e}^{-\frac{(t - t_0^s)}{\tau_s}}, \tag{4}$$

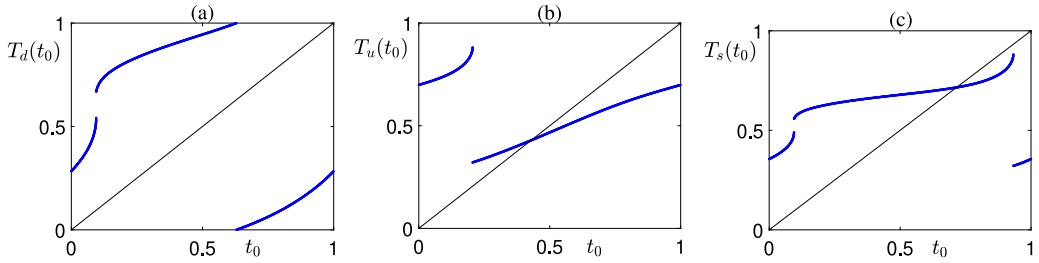

Fig. 2. Illustrative examples of T_j mod 1 for $j = d;\ u;\ s$, with $C(t) = \sin(2\pi t)$, showing behaviour similar to [25]. Parameters: $\tau_w = 0.75,\ \tau_s = 0.25,\ H_0^+ = 0.75,\ H_0^- = 0.1562,\ a^\pm = 0.08675$.

with initial data determined self-consistently by $x_w(t_0^w) = H^-(t_0^w)$ and $x_s(t_0^s) = H^+(t_0^s)$. We denote switching event times on the lower threshold by T_{2i} and those on the upper by T_{2i+1} where $i \in \mathbb{Z}$, $T_{2i} = \inf\{t \mid x(t) = H^-(t);\ t \geq T_{2i-1}\}$ and $T_{2i+1} = \inf\{t \mid x(t) = H^+(t);\ t \geq T_{2i}\}$. See Fig. 1 for an example of the use of this notation.

We note that biological constraints require a monotonically decreasing x_s and a monotonically increasing x_w. Wake and sleep homeostatic pressures asymptote to 1 and 0, respectively, and therefore stay in the interval $(0, 1)$. These restrictions yield $\tau_s > 0$, $\tau_w > 0$, and switching events always exist when

$$a^- < H_0^- < H_0^+ < 1 - a^+. \tag{5}$$

2.1. Circle maps of the two-process model

Nakao et al. [20,21] showed that the dynamics of the two-process model can be studied using one dimensional maps with discontinuities. Using this observation, Bailey et al. [25] introduced three different one dimensional maps in terms of switching event times to study periodic orbits and their bifurcations. These are: (i)– the down map $T_d : \mathbb{R} \to \mathbb{R}$ from upper to lower threshold, i.e. a map that takes a point $(H^+(t_0), t_0)$ on the upper threshold and maps it into the next point on the lower threshold. (ii)– the up map $T_u : \mathbb{R} \to \mathbb{R}$ from lower to upper threshold. Therefore, $T_d(t_0)$ and $T_u(t_0)$ are the first times greater than t_0 such that $x_s(T_d(t_0), t_0) = H^-(T_d(t_0))$ and $x_w(T_u(t_0), t_0) = H^+(T_u(t_0))$ hold. (iii)– the map from upper threshold into itself (composition of the down and up maps) $T_s : \mathbb{R} \to \mathbb{R}$ where $T_s(t_0) = T_u(T_d(t_0))$. The upper and lower thresholds are one day periodic (see Eq. (2)), hence all three maps have the following property

$$T_j(t_0 + 1) = T_j(t_0) + 1, \qquad j = d, u, s. \tag{6}$$

Examples of these maps are illustrated in Fig. 2. In panel (c) the diagonal line helps to see fixed points of the map $T_s(t_0)$ (corresponding to periodic solutions).

The model has various types of periodic orbits and these can be characterised as having p sleep–wake episodes in q days. Thus, t_0 yields a (p, q) periodic orbit if $T_s^p(t_0) = t_0 + q$ where $(T_s^j(t_0) - t_0) \notin \mathbb{N}$ for $j = 1, \ldots, p-1$. If T_s has a (p, q) periodic solution, the greatest common divisor of p and q will be 1 and the theory of monotonic circle maps implies that the function T_s has rational rotation number q/p (cf.[25,31]). An example of a $(1, 1)$ periodic orbit is given in Fig. 1, and more general (p, q) periodic orbits in Fig. 3.

3. Construction and stability of periodic orbits

Similar to [30], we show how to construct a $(1, 1)$ periodic orbit, with the extension to other (p, q) periodic orbits being straightforward.

A $(1, 1)$ periodic solution has period $\Delta = 1$ and contains one wake episode and one sleep episode as illustrated in Fig. 1. To build this orbit let us consider a solution $x_w(t, t_0)$ that starts from the lower threshold at $t = t_0$ with an initial value $x_w(t_0) = x_0$. Since the solution starts at the lower threshold we also have $H^-(t_0) = x_0$. The solution will evolve according to Eq. (3) until it hits the upper threshold at $t = T_1$ with a state value $x_w(T_1) = x_1$. We denote the duration of the wake episode by $\Delta_1 = T_1 - t_0$. At the upper threshold $H^+(T_1) = x_1$ holds and the sleep state starts. Then the solution $x_s(t, T_1)$ will evolve according to Eq. (4) until it hits the lower threshold at $t = 1 + t_0$ with a state value $x_s(T_1 + \Delta_2) = x_2$ where $\Delta_2 = 1 - \Delta_1$ denotes the duration of the sleep episode. At the lower threshold $H^-(t) = x_2$ holds and a switch from sleep to awake occurs. Due to periodicity we also have that $x_2 = x_0$. To complete the procedure we need to determine the unknowns $(t_0, x_0, \Delta_1, x_1, x_2)$ by simultaneously solving a system of five equations:

$$\begin{aligned} &x_0 = H_0^- + a^- C(t_0); \quad x_1 = 1 - (1 - x_0)\mathrm{e}^{-\Delta_1/\tau_w}, \\ &x_1 = H_0^+ + a^+ C(t_0 + \Delta_1); \quad x_2 = x_1 \mathrm{e}^{-(1-\Delta_1)/\tau_s}; \quad x_2 = x_0. \end{aligned} \tag{7}$$

Eqs. (7) are equivalent to conditions 2.30 in [30] for the specific case $p = q = 1$. In practice the unknowns can be found using a numerical routine for the simultaneous solution of a nonlinear system (such as `fsolve` in Matlab), subject to the physical constraint that $0 < \Delta_1 < 1$. In general, to build any (p, q) periodic orbit one needs to solve a system of equations with more unknown parameters; for example to construct a $(2, 3)$ periodic orbit nine equations are required to determine nine unknowns. We illustrate the shape of $(1, 1)$ and $(2, 3)$ periodic orbits in Fig. 4 where we denote the duration of wake and sleep episodes by Δ_{2i+1} and Δ_{2i}, respectively, $i \in \mathbb{Z}$.

Eqs. (7) give conditions for the existence of periodic solutions, but we are also interested in their stability. Since the constructed periodic orbits are solutions of a nonsmooth flow one needs to apply Floquet theory with care. However, there is a growing body of work on nonsmooth systems (existence, uniqueness, stability), and in particular piecewise linear systems, that can be used for this purpose and here we will adapt the approach in [32,33] that is suited to treating periodic solutions with an arbitrary number of switching events. The approach makes use of saltation operators that are able to map perturbations to a periodic orbit through a switching event. Ultimately, we will see that this can also be used to construct a Lyapunov exponent reminiscent of that expected for a smooth dynamical system albeit with a correction term to take into account the jumps encountered at switching events.

3.1. Stability using a nonsmooth flow approach: Floquet exponents

Saltation operators are used to capture the evolution of perturbations through switching events where either the solution or the vector field (or both) has a discontinuity. Some application

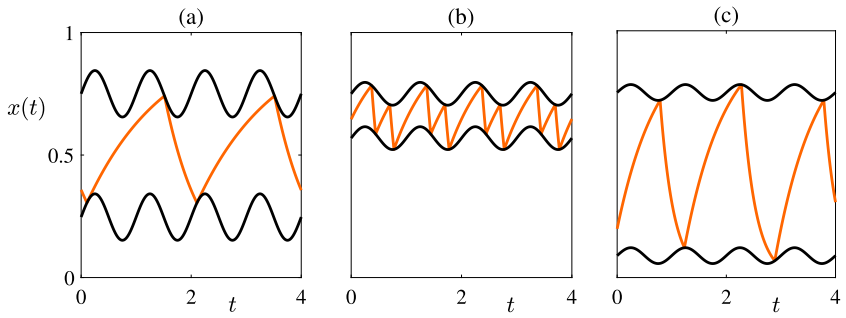

Fig. 3. Periodic solutions of the two-process model with $C(t) = \sin(2\pi t)$. (a) A $(1, 2)$ periodic orbit (one sleep–wake episode in two days). Parameters: $\tau_w = 1.426$, $\tau_s = 0.6634$, $H_0^+ = 0.75$, $H_0^- = 0.2469$, and $a^\pm = 0.09478$. (b) A $(2, 1)$ periodic orbit (two sleep–wake episodes in one day). Parameters: $\tau_w = 0.75$, $\tau_s = 0.25$, $H_0^+ = 0.75$, $H_0^- = 0.569$, and $a^\pm = 0.04659$. (c) A $(2, 3)$ periodic orbit (two sleep–wake episodes in three days). Parameters: $\tau_w = 0.75$, $\tau_s = 0.25$, $H_0^+ = 0.75$, $H_0^- = 0.08883$, and $a^\pm = 0.03213$.

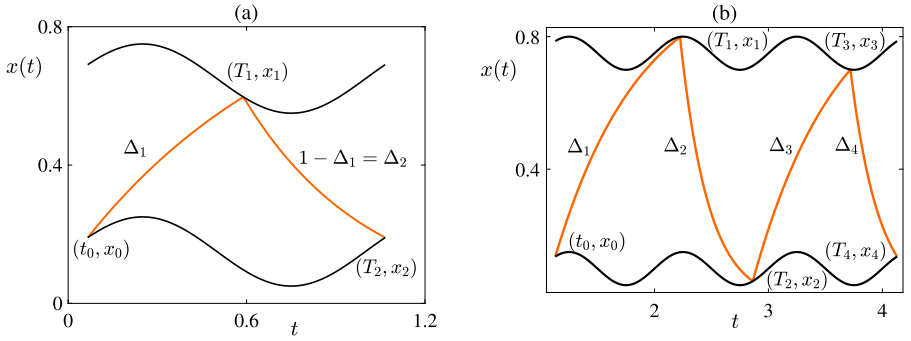

Fig. 4. (p, q) Periodic orbits in the two-process model with $C(t) = \sin(2\pi t)$. (a): A $(1, 1)$-periodic orbit. In order to construct this orbit explicitly, we need to determine $(t_0, x_0, \Delta_1, x_1, x_2)$ from Eqs. (7). Here t_0 is the wake onset time with initial homeostatic sleep pressure x_0, Δ_1 is the duration of the wake episode, x_1 is the value of homeostatic sleep pressure at which switching from wake to sleep occurs, and x_2 is the homeostatic sleep pressure for which switching from sleep to wake occurs. Parameters: $\tau_w = 0.75$, $\tau_s = 0.417$, $H_0^+ = 0.65$, $H_0^- = 0.15$, $a^\pm = 0.1$. (b): A $(2, 3)$-periodic orbit, and to construct this we need to determine nine unknowns $(t_0, x_0, \Delta_1, x_1, \Delta_2, x_2, \Delta_3, x_3, x_4)$. Here we denote $T_1 = t_0 + \Delta_1$, $T_2 = T_1 + \Delta_2$, $T_3 = T_2 + \Delta_3$, $T_4 = t_0 + 3$, and $\Delta_4 = T_4 - T_3$. At the lower threshold, switching from sleep to wake occurs at (t_0, x_0), (T_2, x_2), and (T_4, x_4). At the upper threshold, switching from wake to sleep occurs at (T_1, x_1) and (T_3, x_3). Parameters: $\tau_w = 0.75$, $\tau_s = 0.25$, $H_0^+ = 0.75$, $H_0^- = 0.1$, $a^\pm = 0.05$.

of saltation matrices are reported by Müller [34] to calculate Lyapunov exponents of discontinuous systems, and Fredriksson and Nordmark [35] in the normal form derivation for impact oscillators. In recent years, they have been used to analyse both node and network behaviour of piecewise linear or impacting oscillatory systems [33,36,37]. Here, we use them to treat the stability of nonsmooth periodic orbits of the two-process model with an augmentation of the Floquet theory for smooth systems. Consider a (p, q) periodic orbit $\bar{x}(t)$ of the system (1) and a perturbed solution $\tilde{x}(t) = \bar{x}(t) + \delta x(t)$ for some small perturbation $\delta x(t)$. Then during a wake state when $T_0 < t < T_1$ (or in general between $T_{2i} < t < T_{2i+1}$), $\delta x(t)$ evolves according to

$$\frac{\mathrm{d}}{\mathrm{d}t}\delta x(t) = -\frac{1}{\tau_w}\delta x. \tag{8}$$

During a sleep state when $T_1 < t < T_2$ (or in general between $T_{2i+1} < t < T_{2i+2}$), $\delta x(t)$ evolves according to

$$\frac{\mathrm{d}}{\mathrm{d}t}\delta x(t) = -\frac{1}{\tau_s}\delta x. \tag{9}$$

In the Appendix, we show that the saltation rule to map a perturbation through a switching event on the upper threshold of the two-process model is given by $\delta x(T_{2i+1}^+) = K_1(T_{2i+1})\delta x(T_{2i+1}^-)$, where

$$K_1(T_{2i+1}) = \frac{a^+\dot{C}(T_{2i+1}) + \frac{a^+}{\tau_s}C(T_{2i+1}) + \frac{H_0^+}{\tau_s}}{a^+\dot{C}(T_{2i+1}) + \frac{a^+}{\tau_w}C(T_{2i+1}) + \frac{H_0^+ - 1}{\tau_w}}. \tag{10}$$

Similarly, the saltation rule on the lower threshold is $\delta x(T_{2i}^+) = K_2(T_{2i})\delta x(T_{2i}^-)$, where

$$K_2(T_{2i}) = \frac{a^-\dot{C}(T_{2i}) + \frac{a^-}{\tau_w}C(T_{2i}) + \frac{H_0^- - 1}{\tau_w}}{a^-\dot{C}(T_{2i}) + \frac{a^-}{\tau_s}C(T_{2i}) + \frac{H_0^-}{\tau_s}}. \tag{11}$$

Note that the saltation operators K_1 and K_2 are well defined as long as their denominators are not zero. These denominators take the form $\dot{H}^\pm(T) - \dot{x}(T)$ for an event time T (remembering $x(T) = H^\pm(T)$) so that saltation is not defined whenever the event occurs at a time when the flow is tangential to the threshold. Such tangency points have particular significance and are discussed further below.

In the absence of tangencies, for any (p, q)-periodic solution (p sleep and p wake in q days, $\Delta = q$), after one period of oscillation, a perturbed trajectory evolves according to $\delta x(q) = M\delta x(t_0)$ where

$$M = K_2(T_{2p})\mathrm{e}^{-\frac{\Delta_{2p}}{\tau_s}}K_1(T_{2p-1})\mathrm{e}^{-\frac{\Delta_{2p-1}}{\tau_w}}\ldots K_2(T_2)\mathrm{e}^{-\frac{\Delta_2}{\tau_s}}K_1(T_1)\mathrm{e}^{-\frac{\Delta_1}{\tau_w}}. \tag{12}$$

Here, Δ_i is the time interval given by $\Delta_i = T_{i+1} - T_i$. Hence, the non-trivial Floquet exponent κ, defined by $\mathrm{e}^{\kappa\Delta} = M$, is given by

$$\kappa = \frac{1}{q}\left[-\left(\frac{1}{\tau_w}(\Delta_1 + \Delta_3 + \cdots + \Delta_{2p-1}) + \frac{1}{\tau_s}(\Delta_2 + \Delta_4 + \cdots + \Delta_{2p})\right) + \sum_{j=1}^{p}\ln|K_1(T_{2j-1})| + \ln|K_2(T_{2j})|\right]. \tag{13}$$

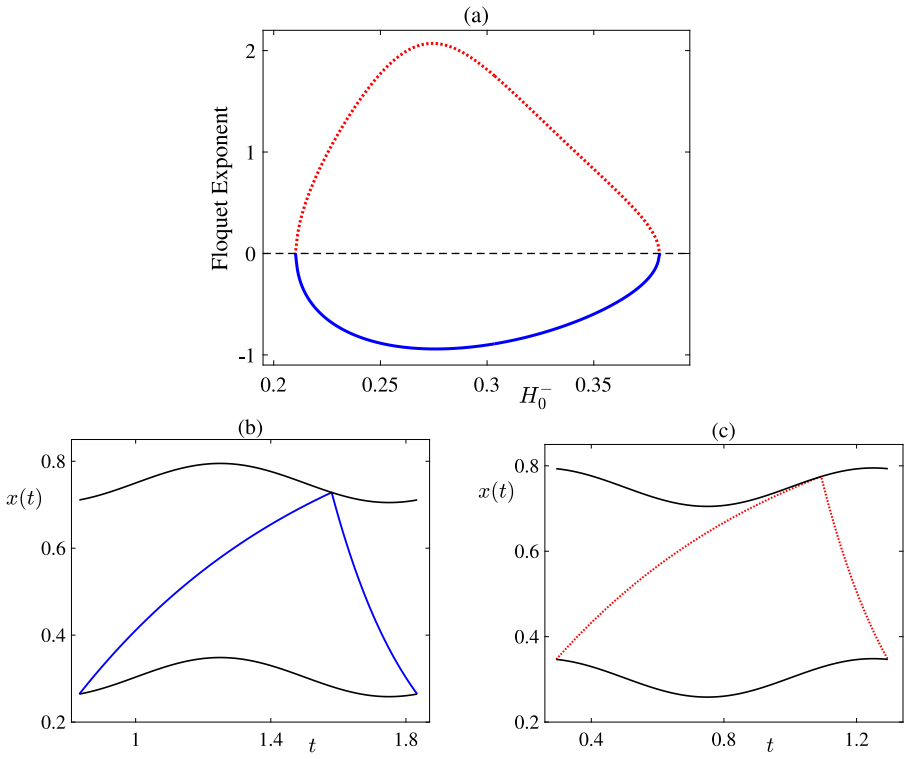

Fig. 5. (a) A bifurcation diagram for $(1,1)$ periodic orbits in the two-process model with $C(t) = \sin(2\pi t)$. When $H_0^- \in (0.2102, 0.381)$ stable (solid blue line) and unstable (dotted red line) periodic solutions coexist. At $H_0^- = 0.2102$ and $H_0^- = 0.381$ these solutions coincide and annihilate each other via saddle–node bifurcation of periodic orbits. Stable (b) and unstable (c) periodic orbits with Floquet exponents -0.8905 and 1.7508, respectively, when $H_0^- = 0.3035$. Parameters: $\tau_w = 0.75,\ \tau_s = 0.25,\ H_0^+ = 0.75,\ a^\pm = 0.04498$.

The periodic orbit will be stable if the Floquet exponent κ has negative real part. For example, in Fig. 4, the $(1,1)$ and $(2,3)$ periodic solutions have $\kappa = -2.73$ and $\kappa = -1.253$, respectively, thus both solutions are stable.

A bifurcation diagram, showing the Floquet exponents of periodic orbits under variation of H_0^- is presented in Fig. 5. At $H_0^- = 0.2102$ and $H_0^- = 0.381$ a saddle–node bifurcation of $(1,1)$ periodic orbits is observed. Examples of stable and unstable periodic orbits are also shown.

3.2. Stability using a map-based approach

In order to calculate the stability of periodic solutions using a map-based approach we first write down implicit expressions for the event times and then consider whether a perturbation to the initial event time grows or decays.

3.2.1. An implicit determination of event times

The trajectories of the two-process model during wake and sleep episodes can be constructed using Eqs. (3) and (4). Moreover, we can make further use of these to develop an implicit relationship between consecutive event times. This effectively gives rise to the map based approach considered in e.g. [20,25]. For a wake episode when $T_{2i} \le t \le T_{2i+1}$, by setting $x_w(t_0^w) = x(T_{2i})$ and $x_w(T_{2i+1}, t_0^w) = x(T_{2i+1})$ in Eq. (3), we find

$$T_{2i+1} + \tau_w \ln|x(T_{2i+1}) - 1| = T_{2i} + \tau_w \ln|x(T_{2i}) - 1|. \tag{14}$$

Using the state values on the upper and lower thresholds, we can rewrite this as

$$\begin{aligned} &T_{2i+1} + \tau_w \ln|H_0^+ + a^+ C(T_{2i+1}) - 1| \\ &= T_{2i} + \tau_w \ln|H_0^- + a^- C(T_{2i}) - 1|. \end{aligned} \tag{15}$$

It is clear from Eq. (15) that T_{2i+1} cannot be explicitly solved in terms of T_{2i}, but we can define an implicit function $G_1(T_{2i}, T_{2i+1}) = 0$ where

$$G_1(T_{2i}, T_{2i+1}) = T_{2i+1} - T_{2i} - \tau_w \ln\left|\frac{H_0^- + a^- C(T_{2i}) - 1}{H_0^+ + a^+ C(T_{2i+1}) - 1}\right|. \tag{16}$$

Moreover, for a sleep episode when $T_{2i+1} \le t \le T_{2i+2}$, from Eq. (4) we have,

$$T_{2i+2} + \tau_s \ln|x(T_{2i+2})| = T_{2i+1} + \tau_s \ln|x(T_{2i+1})|. \tag{17}$$

Using the state values on the upper and lower thresholds, we obtain

$$T_{2i+2} + \tau_s \ln|H_0^- + a^- C(T_{2i+2})| = T_{2i+1} + \tau_s \ln|H_0^+ + a^+ C(T_{2i+1})|. \tag{18}$$

We observe that T_{2i+2} also cannot be explicitly solved in terms of T_{2i+1}, however we can define an implicit function $G_2(T_{2i+1}, T_{2i+2}) = 0$ where

$$G_2(T_{2i+1}, T_{2i+2}) = T_{2i+2} - T_{2i+1} - \tau_s \ln\left|\frac{H_0^+ + a^+ C(T_{2i+1})}{H_0^- + a^- C(T_{2i+2})}\right|. \tag{19}$$

Complete solutions, including periodic orbits, can be found by the simultaneous solution of $G_1(T_{2i}, T_{2i+1}) = 0$ and $G_2(T_{2i+1}, T_{2i+2}) = 0$ For example, a $(1,1)$ periodic orbit is the solution of the two equations $G_1(T_0, T_1) = 0$ and $G_2(T_1, T_0 + 1) = 0$, and see Fig. 1 for a reminder of the event notation. For more general (p,q) orbits the same process applies, though one must now solve $2p+1$ simultaneous equations (with one of these enforcing periodicity). Next we will show how to use these implicit relations to assess the stability of periodic orbits (that do not tangentially intersect $H^\pm$).

3.2.2. An explicit determination of event time stability

Consider a (p, q) periodic orbit that starts from the lower threshold at $t = T_{2i}$ and a perturbed trajectory that starts at the perturbed time $t = T_{2i} + \delta T_{2i}$. The periodic and perturbed solutions reach to the upper threshold at $t = T_{2i+1}$ and $t = T_{2i+1} + \delta T_{2i+1}$, respectively. A first order Taylor expansion of Eq. (16) gives

$$\begin{aligned} &G_1(T_{2i} + \delta T_{2i}, T_{2i+1} + \delta T_{2i+1}) \\ &= G_1(T_{2i}, T_{2i+1}) + \frac{\partial G_1}{\partial T_{2i}}\delta T_{2i} + \frac{\partial G_1}{\partial T_{2i+1}}\delta T_{2i+1}. \end{aligned} \tag{20}$$

Then using $G_1(T_{2i} + \delta T_{2i}, T_{2i+1} + \delta T_{2i+1}) = G_1(T_{2i}, T_{2i+1}) = 0$, we obtain

$$\delta T_{2i+1} = -\frac{\frac{\partial G_1}{\partial T_{2i}}}{\frac{\partial G_1}{\partial T_{2i+1}}}\delta T_{2i} \equiv S_1(T_{2i}, T_{2i+1})\delta T_{2i}, \tag{21}$$

where

$$\begin{aligned} &S_1(T_{2i}, T_{2i+1}) \\ &= \frac{(a^-\tau_w\dot{C}(T_{2i}) + a^-C(T_{2i}) + H_0^- - 1)(H_0^+ + a^+C(T_{2i+1}) - 1)}{(a^+\tau_w\dot{C}(T_{2i+1}) + a^+C(T_{2i+1}) + H_0^+ - 1)\left(H_0^- + a^-C(T_{2i}) - 1\right)} \\ &= \left[\frac{a^-\dot{C}(T_{2i}) + \frac{a^-}{\tau_w}C(T_{2i}) + \frac{H_0^- - 1}{\tau_w}}{a^+\dot{C}(T_{2i+1}) + \frac{a^+}{\tau_w}C(T_{2i+1}) + \frac{H_0^+ - 1}{\tau_w}}\right] \mathrm{e}^{-\frac{T_{2i+1} - T_{2i}}{\tau_w}}. \end{aligned} \tag{22}$$

Similarly, a first order expansion of Eq. (19) yields

$$\begin{aligned} G_2(T_{2i+1} + \delta T_{2i+1}, T_{2i+2} + \delta T_{2i+2}) &= G_2(T_{2i+1}, T_{2i+2}) \\ &+ \frac{\partial G_2}{\partial T_{2i+1}}\delta T_{2i+1} + \frac{\partial G_2}{\partial T_{2i+2}}\delta T_{2i+2}. \end{aligned} \tag{23}$$

Using the fact that $G_2(T_{2i+1} + \delta T_{2i+1}, T_{2i+2} + \delta T_{2i+2}) = G_2(T_{2i+1}, T_{2i+2}) = 0$, we obtain

$$\delta T_{2i+2} = -\frac{\frac{\partial G_2}{\partial T_{2i+1}}}{\frac{\partial G_2}{\partial T_{2i+2}}}\delta T_{2i+1} \equiv S_2(T_{2i+1}, T_{2i+2})\delta T_{2i+1}, \tag{24}$$

where

$$\begin{aligned} &S_2(T_{2i+1}, T_{2i+2}) \\ &= \frac{(a^+\tau_s\dot{C}(T_{2i+1}) + a^+C(T_{2i+1}) + H_0^+)(H_0^- + a^-C(T_{2i+2}))}{(a^-\tau_s\dot{C}(T_{2i+2}) + a^-C(T_{2i+2}) + H_0^-)(H_0^+ + a^+C(T_{2i+1}))} \\ &= \left[\frac{a^+\dot{C}(T_{2i+1}) + \frac{a^+}{\tau_s}C(T_{2i+1}) + \frac{H_0^+}{\tau_s}}{a^-\dot{C}(T_{2i+2}) + \frac{a^-}{\tau_s}C(T_{2i+2}) + \frac{H_0^-}{\tau_s}}\right] \mathrm{e}^{-\frac{T_{2i+2} - T_{2i+1}}{\tau_s}}. \end{aligned} \tag{25}$$

Hence for a (p, q) periodic orbit we have $\delta T_{2p} = \mu\delta T_0$ where

$$\mu = S_2(T_{2p-1}, T_{2p})S_1(T_{2p-2}, T_{2p-1})\ldots S_2(T_1, T_2)S_1(T_0, T_1). \tag{26}$$

Thus the periodic orbit is stable when $|\mu| < 1$. We note that Eq. (25) is the same as that derived by explicit differentiation of the map in [30]. Furthermore, as expected, for a given periodic orbit, both the nonsmooth flow method leading to the Floquet exponent (13) and the expression for stability from the map-based approach in (26) are equivalent. To clarify this last point a little further see the *intermezzo* below which also includes a specific example. In addition to periodic solutions, quasiperiodic solutions and chaos may also be possible in the two-process model. It is therefore instructive to construct the Lyapunov exponent.

Intermezzo: equivalence between nonsmooth flow and map approaches

Here, we clarify how M in Eq. (12) and μ in Eq. (26) are equivalent. Note that K_1 is a function of T_{2i+1} (upper boundary switching times) and prescribes how a perturbation to the orbit is mapped across the upper switching boundary. Similarly K_2 is a function of T_{2i} (lower boundary switching times). These factors, included in (12), reflect the effect of a discontinuous change in the vector field for the linear stability calculation of a periodic orbit. The remaining exponential factors describe the (linearised) evolution of a perturbed flow between events. Simply put, in the nonsmooth flow perspective, M determines how an initial perturbation to a periodic orbit changes over one period. In the map based approach, linear stability is determined by computing the evolution of perturbations in the event times. To achieve this we used Eqs. (21) and (24), which involve the multiplicative factors $S_{1,2}$, which are themselves functions of event times. For example, S_1 is a function of (T_{2i}, T_{2i+1}) as given by Eq. (22). The exponential term in this equation corresponds to linear evolution of a perturbation during the wake state in the nonsmooth flow approach. The numerator of the coefficient in the equation is a function of T_{2i} and the denominator is a function of T_{2i+1}. Similarly, S_2 is a function of (T_{2i+1}, T_{2i+2}) and explicitly given by Eq. (25). The exponential term in this equation corresponds to the linear evolution of a perturbation during the sleep state in the nonsmooth flow approach. The numerator of the coefficient in the equation is a function of T_{2i+1} and the denominator is a function of T_{2i+2}. However, we compute saltation operators either on an upper boundary (with switching time T_{2i+1}, where we use $K_1(T_{2i+1})$) or on a lower boundary (with switching time T_{2i}, where we use $K_2(T_{2i})$). Therefore, their numerator and denominator are either a function of T_{2i+1} or T_{2i}. As a result of this, although both approaches have the same expression for the denominator their numerators are swapped (S_1 and K_2 have same numerator, and S_2 and K_1 have same numerator). To compute stability, we multiply these terms over a period, and hence we conclude M and μ are equivalent. To see this more explicitly, consider, for example, a (1, 1) periodic orbit with event times T_0, T_1, T_2. Using the nonsmooth flow approach one finds

$$\begin{aligned} M &= K_2(T_2)\mathrm{e}^{-\frac{\Delta_2}{\tau_s}}K_1(T_1)\mathrm{e}^{-\frac{\Delta_1}{\tau_w}} \\ &= \frac{a^-\dot{C}(T_2) + \frac{a^-}{\tau_w}C(T_2) + \frac{H_0^- - 1}{\tau_w}}{a^-\dot{C}(T_2) + \frac{a^-}{\tau_s}C(T_2) + \frac{H_0^-}{\tau_s}} \\ &\quad\times \mathrm{e}^{-\frac{\Delta_2}{\tau_s}}\frac{a^+\dot{C}(T_1) + \frac{a^+}{\tau_s}C(T_1) + \frac{H_0^+}{\tau_s}}{a^+\dot{C}(T_1) + \frac{a^+}{\tau_w}C(T_1) + \frac{H_0^+ - 1}{\tau_w}}\mathrm{e}^{-\frac{\Delta_1}{\tau_w}}. \end{aligned} \tag{27}$$

Using the map based approach one finds

$$\begin{aligned} \mu &= S_2(T_1, T_2)S_1(T_0, T_1) \\ &= \frac{a^+\dot{C}(T_1) + \frac{a^+}{\tau_s}C(T_1) + \frac{H_0^+}{\tau_s}}{a^-\dot{C}(T_2) + \frac{a^-}{\tau_s}C(T_2) + \frac{H_0^-}{\tau_s}} \\ &\quad\times \mathrm{e}^{-\frac{\Delta_2}{\tau_s}}\frac{a^-\dot{C}(T_0) + \frac{a^-}{\tau_w}C(T_0) + \frac{H_0^- - 1}{\tau_w}}{a^+\dot{C}(T_1) + \frac{a^+}{\tau_w}C(T_1) + \frac{H_0^+ - 1}{\tau_w}}\mathrm{e}^{-\frac{\Delta_1}{\tau_w}}. \end{aligned} \tag{28}$$

From the periodicity of the orbit and of $C(t)$, $T_2 = T_0 + 1$, $C(T_2) = C(T_0 + 1) \equiv C(T_0)$ and $\dot{C}(T_2) = \dot{C}(T_0 + 1) \equiv \dot{C}(T_0)$, it can be seen that (27) and (28) are equal. Similarly, this equivalence of M and μ can be established for any (p, q) periodic orbit.

4. Lyapunov exponents

Lyapunov exponents quantify the exponential rates of convergence or divergence of initially close orbits of an attractor in state space and are useful to determine regions of parameter space with different emergent behaviour. Periodic attractors have non-positive exponents whereas chaotic attractors have at least one positive Lyapunov exponent.

For a general dynamical system $\dot{x} = f(x),\ x \in \mathbb{R}^n$, the spectrum of the Lyapunov exponents, λ_i, is given for some different initial conditions $\delta x_i(t_0)$, as:

$$\lambda_i = \lim_{t\to\infty} \frac{1}{t-t_0} \ln \frac{||\delta x(t)||}{||\delta x_i(t_0)||}, \qquad i = 1, \ldots, n, \tag{29}$$

where $\delta x(t)$ indicates evolution of the distance $\bar{x}(t) - \tilde{x}(t)$ between $\bar{x}(t)$ and the perturbed trajectory $\tilde{x}(t)$ with an initial condition $\bar{x}(t_0) + \delta x(t_0)$. For smooth continuous dynamical systems, Lyapunov exponents are generally computed by solving a variational equation where the Jacobian of the system is evaluated along an orbit. Indeed, algorithms for computing the Lyapunov exponents of smooth continuous systems are well developed [38–40]. However, these classical algorithms cannot be directly applied to compute Lyapunov exponents of nonsmooth dynamical systems. As we have shown in Section 3.1, the evaluation of the variational equation of a nonsmooth system requires careful consideration. Here we develop the notion of Lyapunov exponent for the two-process model, by re-visiting techniques originally applied in the analysis of impacting systems [34,41].

Similar to the derivation of Eq. (12), for any arbitrary time t, the overall deviation between two trajectories $\bar{x}(t)$ and $\tilde{x}(t)$ of the two-process model, assuming a common pattern of close threshold crossings, can be written as

$$\delta x(t) = \mathrm{e}^{-\frac{(t-\Delta_k)}{\tau_w}} K_2(T_k) \mathrm{e}^{-\frac{\Delta_k}{\tau_s}} K_1(T_{k-1}) \mathrm{e}^{-\frac{\Delta_{k-1}}{\tau_w}} \ldots K_1(T_1) \mathrm{e}^{-\frac{\Delta_1}{\tau_w}} \delta x(t_0), \tag{30}$$

where $K_1(t)$ and $K_2(t)$ are saltation rules given by Eqs. (10) and (11), respectively. Here, $\Delta_k = T_{k+1} - T_k$. Thus using formula (29) along with Eq. (30), we can formulate the Lyapunov exponent of the two-process model as

$$\begin{aligned}
\lambda &= \lim_{k\to\infty} \frac{1}{T^k - T^0} \\
&\quad \times \ln \left| \prod_{j=1}^{k} K_\mu(T_j) \mathrm{e}^{-\frac{1}{\tau_w}(\Delta_1+\Delta_3+\cdots+\Delta_{k-1})} \mathrm{e}^{-\frac{1}{\tau_s}(\Delta_2+\Delta_4+\cdots+\Delta_k)} \right| \\
&= \lim_{k\to\infty} \frac{1}{T^k - T^0} \left[-\frac{1}{\tau_w}(\Delta_1 + \Delta_3 + \cdots + \Delta_{k-1}) \right. \\
&\quad \left. + -\frac{1}{\tau_s}(\Delta_2 + \Delta_4 + \cdots + \Delta_k) + \sum_{j=1}^{k} \ln |K_\mu(T_j)| \right],
\end{aligned} \tag{31}$$

where $\mu = 1$ if j is odd and $\mu = 2$ if j is even. Here we consider the trajectory $\bar{x}(t)$ to start from the lower threshold but a similar formula can easily be obtained when it starts from the upper threshold. We note that there are two contributions to λ, one from the smooth flow during sleep and wake episodes and the other from the discontinuous nature of the switching mechanism at threshold crossings. Note that the restriction to 'common pattern' means that events are neither created or destroyed by perturbation. This is violated in a nonsmooth grazing bifurcation (and see Section 5). Nonetheless, even excluding this scenario from the construction of the Lyapunov exponent still gives a test for chaos ($\lambda > 0$).

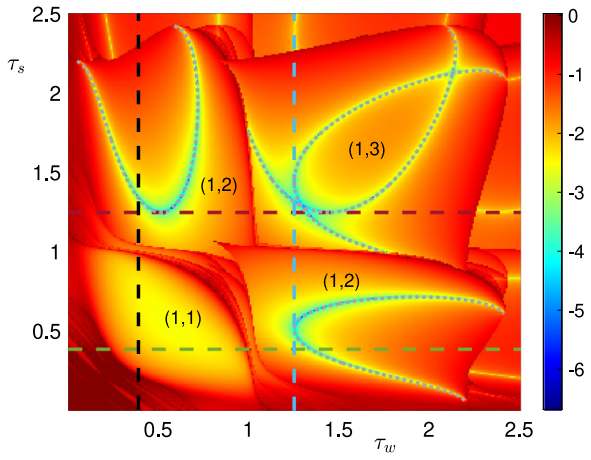

Fig. 6. Lyapunov exponent diagram in the (τ_w, τ_s) plane for the two-process model with $C(t) = \sin(2\pi t)$ and $a^{\pm} = a$. The $(1, 1)$, $(1, 2)$ and $(1, 3)$ periodic orbits occupy large regions of parameter space. Tangencies on the lower threshold occur above the line $\tau_s = \tau_s^-$ (dashed green line). Tangencies on the upper threshold occur to the right of the line $\tau_w = \tau_w^+$ (dashed black). The down map is non-monotonic above the line $\tau_s = \tau_s^+$ (dashed brown). The up map is non-monotonic to the right of the line $\tau_w = \tau_w^-$ (dashed light blue). There is no signature of chaos since $\lambda \leq 0$ across the whole plane. The dotted grey lines track out the locus of super-stable $(1, 2)$ and $(1, 3)$ cycles. Parameters: $H_0^- = 0.25$, $H_0^+ = 0.75$, $a = 0.09478$.

The numerical determination of the Lyapunov exponent is performed with a second order Runge–Kutta scheme for time-stepping the two-process model with a small fixed step size and a linear interpolation between states immediately above and below the threshold to give a more accurate determination of the event time. This event time is then used as the initial time for the next forward evolution of the model, with initial data constructed from extrapolation of the state just below threshold to the event time, and the process repeated. We depict a Lyapunov exponent diagram for the two-process model in the (τ_w, τ_s) parameter plane calculated in this fashion in Figs. 6 and 8 for two different parameter regimes. On Figs. 6 and 8 we also add lines that denote structural changes in the map, namely lines that mark transitions from a continuous circle map to a map with at least one gap and lines that mark transitions from a monotonic circle map to a nonmonotonic circle map. Specifically, as recognised in [30] and generalised in [24], transitions to gaps occur when either $x_w(t)$ is tangential to the upper threshold or $x_s(t)$ is tangential to the lower threshold. Whereas transitions from monotonicity to nonmonotonicity occur when either $x_w(t)$ is tangential to the lower threshold or $x_s(t)$ is tangential to the upper threshold. For the case that $C(t) = \sin(2\pi t)$ (or $C(t) = \cos(2\pi t)$) and $a^{\pm} = a$ it can be shown (using elementary trigonometric identities) that the transition to maps with gaps occur when $\tau_w \geq \tau_w^+ \equiv \sqrt{(1-H_0^+)^2 - a^2}/(2a\pi)$, and when $\tau_s \geq \tau_s^- \equiv \sqrt{(H_0^-)^2 - a^2}/(2a\pi)$. Whereas the transition from monotonicity to nonmonotonicity occur when $\tau_w \geq \tau_w^- \equiv \sqrt{(1-H_0^-)^2 - a^2}/(2a\pi)$ (non-monotonicity in the up-map), or when $\tau_s \geq \tau_s^+ \sqrt{(H_0^+)^2 - a^2}/(2a\pi)$ (non-monotonicity in the down-map).

We note that although the underlying circle map was non-monotonic for some regions of the parameter space shown in Figs. 6 and 8 no regions where $\lambda > 0$, indicative of chaos, were found. We can however easily identify lines in the colour plots that track out local minima of the Lyapunov exponent, which are the locus of super-stable cycles. Using Eq. (26) these are defined by the condition $\mu = 0$.

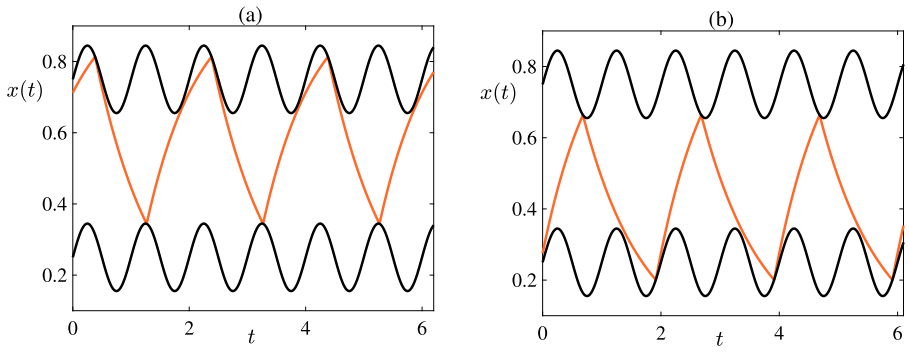

Fig. 7. An example of bistability in the two-process model at the point $(\tau_w, \tau_s) = (0.887, 1.029)$ in Fig. 6. (a) A stable $(1, 2)$ orbit with Lyapunov exponent $\lambda = -0.8166$ obtained using initial data $x(0) = 0.71$. (b) A stable $(1, 2)$ orbit with Lyapunov exponent $\lambda = -1.5531$ obtained using initial data $x(0) = 0.27$.

Finally, we note that in [30], a symmetry

$$(t, x_s; \tau_s, H_0^+, H_0^-, a, t_0) \mapsto (t+1/2,\ 1-x_w;\ \tau_w,\ 1-H_0^-,\ 1-H_0^+,\ a,\ t_0+1/2) \tag{32}$$

was identified. This symmetry explains the approximate reflection symmetry about the diagonal line in Fig. 6. The symmetry is not exact, for example in the neighbourhood of $\tau_s = \tau_w = 1$, because there are small regions of bistability and although the parameters $\tau_s, \tau_w, H_0^+, H_0^-$ and a respect the symmetry condition (32), the initial conditions used to calculate Fig. 6 did not. An example of two co-existing stable $(1, 2)$ orbits is shown in Fig. 7.

Although non-monotonicity of the map is a prerequisite for chaos (say via a period-doubling cascade) and parameters for non-monotonicity are easily identified in Fig. 6 for the two-process model, with $C(t) = \sin(2\pi t)$, we did not find any signature of chaos (positive Lyapunov exponent). A similar observation was found for the choice $C(t) = \cos(2\pi t)$ made in Fig. 8 (using parameters from Fig. 2 in [42]).

5. Bifurcations of periodic solutions

In [25,30], using the circle map framework the bifurcation structure of the two-process model was investigated. This led to a bifurcation set consisting of an Arnol'd tongue-like structure. At small circadian amplitudes a, regions of existence of periodic solutions were bounded by saddle–node bifurcations. At higher amplitudes, in regions where the underlying circle map was not continuous, periodic solutions could in addition be created/destroyed by border collision bifurcations. In terms of the flow, these border collisions were associated with periodic orbits in which either $x_w(t)$ was tangential to the upper threshold or $x_s(t)$ was tangential with the lower threshold. Two types of border collision could occur, termed Type I and Type II in [25], as illustrated in Figs. 9 and 10. Type I border collisions yield the creation/destruction of an unstable fixed point and occur when a fixed point of the map coincides with the side of the gap where the derivative of the map is infinite. This corresponds to periodic orbits of the model such that the homeostatic sleep pressure switches at a tangency point. Type II border collisions result in creation/annihilation of either an unstable or a stable fixed point and occur when a fixed point of the map coincides with the side of the gap where the derivative is finite. This corresponds to periodic orbits in the two process model such that the homeostatic sleep pressure bypasses the tangency point and switches at a later time.

Details of how to construct the saddle–node bifurcations from the map-based approach and how to find Type I and Type II grazing bifurcations are given in [30]. Here we demonstrate how to calculate the saddle–node bifurcations from the nonsmooth

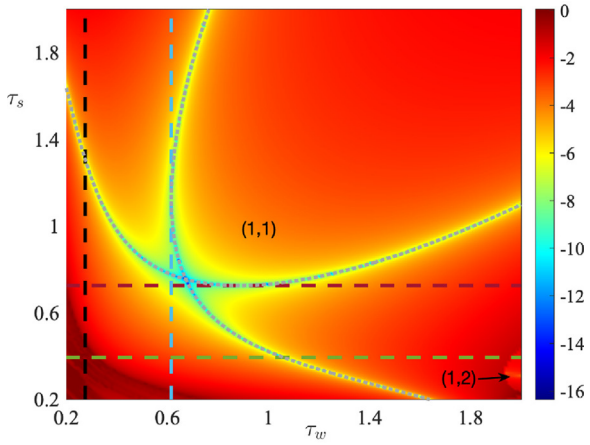

Fig. 8. Lyapunov exponent diagram in the (τ_w, τ_s) plane for the two-process model with $C(t) = \cos(2\pi t)$ and $a^{\pm} = a$. The $(1, 1)$ and $(1, 2)$ periodic orbits occupy large regions of parameter space. Tangential crossings of the lower threshold occur above the line $\tau_s = \tau_s^-$ (dashed green line). Tangential crossings of the upper threshold occur to the right of the line $\tau_w = \tau_w^+$ (dashed black). The down map is non-monotonic above the line $\tau_s = \tau_s^+$ (dashed brown). The up map is non-monotonic to the right of the line $\tau_w = \tau_w^-$ (dashed light blue). There is no signature of chaos since $\lambda \leq 0$ across the whole plane. The dotted grey lines track out the locus of super-stable $(1, 1)$ cycles. Parameters: $H_0^- = 0.4$, $H_0^+ = 0.7$, $a = 0.15$.

flow. Using a method analogous to that used by [30], we also demonstrate how to find grazing bifurcations. In addition, we use our nonsmooth Lyapunov flow method to provide further insight to the Arnol'd tongue-like bifurcation structure found in [25,30].

5.1. Saddle–node bifurcations

Here we use results from Section 3 to determine Arnol'd tongue structures for the regions in parameter space where stable and unstable (p, q) periodic orbits co-exist. At the tongue borders the following two conditions must hold: (i) a (p, q) periodic solution must exist, and (ii) the Floquet exponent of the orbit must be zero (since stable and unstable periodic solutions intersect). To illustrate this method we will construct saddle–node bifurcation boundaries of $(2, 3)$ periodic orbits. In order to construct a $(2, 3)$ periodic solution that starts from the lower threshold we need to determine nine unknowns $(t_0, x_0, \Delta_1, x_1, \Delta_2, x_2, \Delta_3, x_3, x_4)$ where (t_0, x_0) is the initial condition, Δ_1, Δ_3 (Δ_2, Δ_4) are duration of awake (sleep) episodes, x_1, x_3 (x_2, x_4) are state values at the upper (lower) threshold crossing, and at the saddle–node bifurcation points the orbit must have $\kappa = 0$ (a zero Floquet exponent). For example, using formula (13), the Floquet exponent of a $(2, 3)$

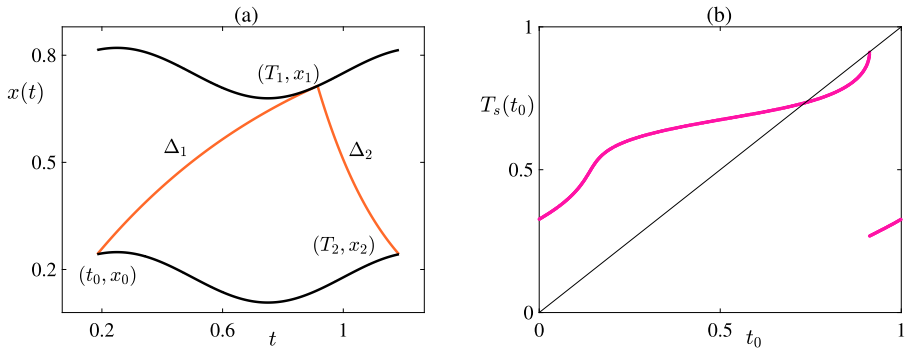

Fig. 9. Type I grazing with $C(t) = \sin(2\pi t)$ and $\tau_w = 0.75$, $\tau_s = 0.25$, $H_0^+ = 0.75$. (a) An example of a Type I grazing of a $(1, 1)$ periodic solution where (t_0, x_0) is the initial value, $\Delta_1(\Delta_2)$ the duration of awake (sleep) episodes, (T_1, x_1) $((T_2, x_2))$ are switching times and states on the upper (lower) threshold. The orbit tangentially intersects with the upper threshold and at the tangency point a transition from wake to sleep state occurs. For $H_0^- = 0.178$ we find $a = 0.0706$ with Floquet exponent $\kappa = 24.5159$ (and hence the periodic orbit is unstable). (b) For the same parameter values we build the one dimensional map with gap. The unstable fixed point of the map coincides with the side of the gap where the derivative of the map is infinite.

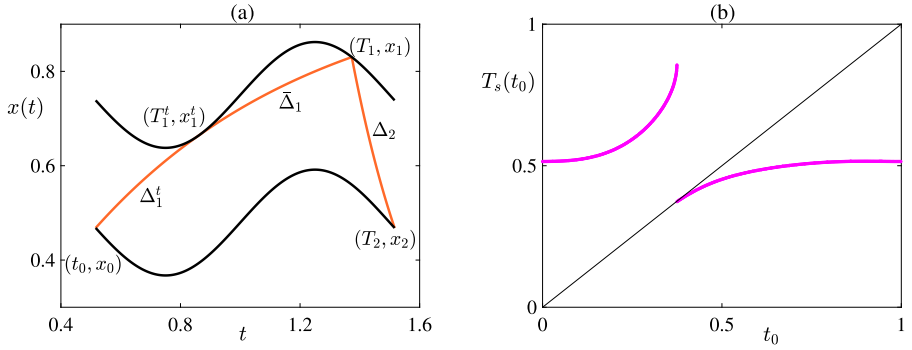

Fig. 10. Type II grazing with $C(t) = \sin(2\pi t)$ and $\tau_w = 0.75$, $\tau_s = 0.25$, $H_0^+ = 0.75$. (a) An example of a Type II grazing $(1, 1)$ periodic solution where (t_0, x_0) is the initial value, Δ_1^t, $\bar{\Delta}_1(\Delta_2)$ the duration of awake (sleep) episodes, (T_1, x_1) $((T_2, x_2))$ are switching times and states on the upper (lower) threshold. (T_1^t, x_1^t) is the tangency point on the upper threshold where the orbit passes through this point continuously without switching. For $H_0^- = 0.4809$ we find $a = 0.1121$ with Floquet exponent $= -0.27991$ (and hence the periodic orbit is stable). (b) For the same parameter values we build the one dimensional map with gap. The stable fixed point of the map coincides with the side of the gap where the derivative of map is finite.

periodic orbit is

$$\kappa = \frac{1}{3}\left[-\left(\frac{1}{\tau_w}(\Delta_1+\Delta_3)+\frac{1}{\tau_s}(\Delta_2+\Delta_4)\right) + \ln|K_1(T_1)K_1(T_3)K_2(T_2)K_2(T_4)|\right]. \tag{33}$$

We will determine the saddle–node bifurcations of the $(2, 3)$ periodic orbit on the (H_0^-, a) plane, treating H_0^- as a bifurcation parameter and computing a using the final condition $\kappa = 0$. Hence at each saddle–node bifurcation point we need to determine ten unknowns $(t_0, x_0, \Delta_1, x_1, \Delta_2, x_2, \Delta_3, x_3, x_4, a)$ by solving the following ten equations simultaneously

$$\begin{aligned}
&x_0 = H_0^- + aC(t_0); \quad x_1 = 1-(1-x_0)e^{-\Delta_1/\tau_w},\\
&x_1 = H_0^+ + aC(T_1); \quad x_2 = x_1 e^{-\Delta_2/\tau_s},\\
&x_2 = H_0^- + aC(T_2); \quad x_3 = 1-(1-x_2)e^{-\Delta_3/\tau_w},\\
&x_3 = H_0^+ + aC(T_3); \quad x_4 = x_3 e^{-\Delta_4/\tau_s},\\
&x_4 = x_0; \quad \kappa = 0.
\end{aligned} \tag{34}$$

To build tongue borders of the $(2, 3)$ periodic orbit, we may then simply perform a numerical continuation that follows the solution path of a with variation in H_0^-. This method is readily adapted to construct the saddle–node bifurcation (tongue border) for any (p, q) periodic orbit. We note that a tongue border defined by saddle–node bifurcations ceases to exist when the saddle–node bifurcation collides with a type II border collision, as discussed in [25].

The equivalent map-based approach used in [25] for computing saddle–node bifurcations requires simultaneously solving the equations for a period-orbit, along with the condition that the derivative of the map at the fixed point corresponding to the periodic orbit has gradient 1, i.e., for the $(2, 3)$ example given above, solving Eqs. (34) but replacing the condition $\kappa = 0$ with $\mu = 1$.

5.2. Type I grazing bifurcation

The necessary conditions for a Type I grazing bifurcation at the upper (lower) threshold of a (p, q) periodic orbit are: (i) a (p, q) periodic solution must exist, and (ii) the homeostatic sleep pressure on wake (sleep) state must switch to sleep (wake) state at the tangency point. This corresponds to the denominators in (10) and (11) vanishing (so that saltation operators are not defined at grazing events). To determine Type I grazing bifurcations of a (p, q) periodic solution we (numerically) simultaneously solve the equations that are needed to build the orbit and the equation that holds at the tangency point. For example, to determine a Type I grazing bifurcations of a $(1, 1)$ periodic orbit we would simultaneously solve the five equations described by Eq. (7) together with the further tangency condition at the upper threshold, $(1 - x_1)/\tau_w = a\dot{C}(t_0 + \Delta_1)$, to determine the six unknowns $(t_0, x_0, \Delta_1, x_1, x_2, a)$. In the left panel of Fig. 9 we illustrate a Type I grazing $(1, 1)$ periodic orbit obtained in this fashion. In the right panel of Fig. 9, we build the corresponding

one dimensional map with a gap where an unstable fixed point of the map coincides with the side of the gap where the derivative of map is infinite. Utilising similar methods, we can determine Type I grazing solutions of any (p, q) periodic orbit.

5.3. Type II grazing bifurcation

The necessary conditions for a Type II grazing bifurcation at the upper (lower) threshold of a (p, q) periodic solution are: (i) a (p, q) periodic solution must exist, and (ii) the homeostatic sleep pressure on wake (sleep) state must continuously passes through the tangency point without switching. Similar to the description in Section 5.2, in order to determine Type II grazing bifurcations of a (p, q) periodic solution we simultaneously solve the equations needed to build the orbit and the equation that holds at the tangency point.

To shed light on this method we show how to determine a Type II grazing bifurcation of a $(1, 1)$ periodic orbit. For an orbit starting from the lower threshold we determine the unknowns $(t_0, x_0, \Delta_1^t, x_1^t, \bar{\Delta}_1, x_1, x_2, a)$, by simultaneously solving

$$\begin{aligned} &x_0 = H_0^- + aC(t_0); \qquad x_1^t = 1-(1-x_0)\mathrm{e}^{-\Delta_1^t/\tau_w},\\ &x_1^t = H_0^+ + aC(T_1^t); \qquad \left(1-x_1^t\right)/\tau_w = a\dot{C}(T_1^t),\\ &x_1 = 1-(1-x_1^t)\mathrm{e}^{-\bar{\Delta}_1/\tau_w}; \quad x_1 = H_0^+ + aC(T_1),\\ &x_2 = x_1\mathrm{e}^{-\Delta_2/\tau_s}; \qquad\qquad x_2 = x_0. \end{aligned} \tag{35}$$

We recognise the collection of equations above as essentially those given in (7) subject to two further constraints defining the tangency condition at (Δ_1^t, x_1^t). In the left panel of Fig. 10 we depict a Type II grazing of a $(1, 1)$ periodic solution obtained in this fashion. In the right panel of Fig. 10, we illustrate the corresponding one dimensional map with gap where a stable fixed point of the map coincides with the side of the gap where the derivative of map is finite. Similarly, we can use this approach to determine Type II grazing solutions of any (p, q) periodic orbit.

Note that the saltation approach cannot be used to determine the stability of a grazing orbit, since saltation factors are not defined at tangencies (their denominators vanish). Nonetheless determining the stability of solutions close to the points in parameter space where grazes occur is not problematic.

5.4. Arnol'd tongue structure

The saddle–node and grazing bifurcations described above can combine to give a bifurcation set consisting of Arnol'd tongues, of the type illustrated in Fig. 11. In this figure, the tongue borders and the Lyapunov exponent are calculated from the nonsmooth flow (not the associated map). We note that for the $(1, 1)$ and $(2, 1)$ tongues shown, Type I and Type II grazing bifurcations occur due to a tangency at the upper threshold only. However, for the $(2, 3)$ tongue Type I (Type II) grazing bifurcations occur due to a tangency at the lower (upper) threshold.

To further explain the bifurcation of periodic solutions we also label some regions inside and outside of the $(1, 1)$ tongue boundaries in Fig. 11. Inside the region (c) a stable and unstable periodic orbit coexist. While moving from region (c) to (b) and (c) to (e) along the solid black curve, periodic orbits are annihilated via a saddle–node bifurcation (as illustrated in Fig. 5). Moving from region (c) to (d) along the white dashed curve, Type II grazing bifurcations occur due to a tangency with the upper threshold and unstable periodic solutions are lost. Moving from region (c) to (d) along the grey dashed curve, Type I grazing bifurcations occur due to a tangency with the upper threshold and unstable periodic solutions are lost. Moving from region (d) to (e) along the solid white curve, Type II grazing bifurcations occur as a result of a tangency with the upper threshold and stable periodic solutions are lost. Hence, inside the region (d) only stable periodic orbits exist, and in regions (b) and (e) there is no $(1, 1)$ periodic solution.

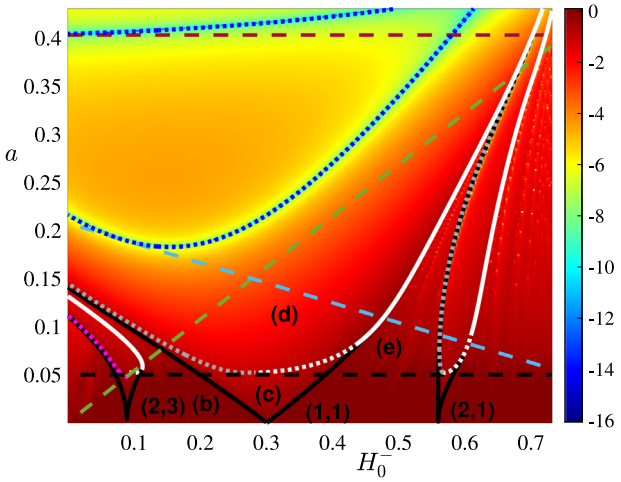

Fig. 11. Arnol'd tongue structure for the two-process model with $C(t) = \sin(2\pi t)$ in the (H_0^-, a) parameter plane. Bifurcation curves for the largest tongues are shown on top of the colour coded Lyapunov exponent λ, and a good correspondence is observed at predicted tongue boundaries (where $\lambda = 0$). Tangencies on the upper threshold occur above the dashed black line which is given by $a = (1 - H_0^+)/(\sqrt{4\pi^2\tau_w^2 + 1})$. Tangencies on the lower threshold occur above the dashed green line given by $a = H_0^-/\sqrt{4\pi^2\tau_s^2 + 1}$. The up map is non-monotonic above the dashed light blue line $a = (1-H_0^-)/\sqrt{4\pi^2\tau_w^2 + 1}$. The down map is non-monotonic above the dashed brown line $a = H_0^+/\sqrt{4\pi^2\tau_s^2 + 1}$. For small circadian amplitude, a the boundaries of Arnol'd tongues are determined by saddle–node bifurcations only and are shown with solid black curves. With increasing a the right branch of each tongue comes to an end, and the extension of these, defined by a grazing bifurcation, are shown with solid white curves. Inside each tongue, Type I and Type II grazing bifurcations form a U-shaped region. Type I grazing bifurcations occur at the left boundary of a U-shaped region (dashed grey and magenta curves) and Type II grazing bifurcations occur at the right boundary (dashed and solid white curves). Grazing bifurcations that occur due to a tangency on the upper threshold are depicted in white and grey and those emerging due to a tangency on the lower threshold are shown in magenta. Solid black curves show saddle–node bifurcations. Dashed white (grey) curves demonstrate Type II (Type I) grazing bifurcations due to a tangency with the upper threshold where unstable periodic solutions are lost. Solid white curves depict Type II grazing bifurcations due to a tangency with the upper threshold where stable periodic solutions are lost. Inside the region (c) the model supports both stable and unstable periodic orbits. In region (d) only stable solutions occur. In region (d), the dashed blue curve shows the parameters that yield a $(1, 1)$ super-stable cycle. The model does not have any $(1, 1)$ periodic solutions in region (b) and (e). We refer to Fig. 8 in [25] for a similar bifurcation diagram built from a purely map based approach. Other parameters: $\tau_w = 0.75$, $\tau_s = 0.25$, $H_0^+ = 0.75$.

The particular bifurcation set shown in Fig. 11 is similar to that shown in Figure 8 of [25] but with two important additions. Firstly the bifurcation set has been shaded according to the value of the Lyapunov exponent. Secondly, the parameter regime has been extended from $a \in [0, 0.2]$ to $a \in [0, 0.4]$. Shading according to the value of the Lyapunov exponent highlights regions of super-stable orbits. For further clarity, lines in parameter space where super-stable orbits exist have been drawn in dashed blue. Note that the maps for parameters supporting super-stable solutions are relatively flat, so that all initial conditions quickly evolve to the fixed point. As shown in [25], stable, periodic orbits exist for all values in the (H_0^-, a) parameter space. Moving across the tongue boundaries shown in Fig. 11 leads to other stable periodic orbits and the bifurcations of these orbits follow a structure that can be described by a Farey sequence, as discussed by Bailey et al. [25].

6. Discussion and future work

Sleep is fundamental for the maintenance of mental health, body functioning and cognitive performance, but many aspects of the sleep–wake mechanism still need further investigation, and mathematical modelling has a significant role to play [17,43]. The two-process sleep model of Borbély remains to this day one of the dominant mathematical models for studying circadian and homeostatic processes underlying sleep–wake regulation. Its properties have recently been re-examined using an event based approach by Bailey et al. [25], emphasising the interesting dynamics that can arise in *maps with gaps*. Here, we have shown that a direct analysis of the underlying nonsmooth flow, from which the event based description arises, is also possible.

Viewing the two-process model as a nonsmooth flow allows for a simple numerical implementation using standard methods for the numerical solution of ordinary differential equations, augmented to detect and adjust for threshold crossings. This circumvents the computational task to construct a one-dimensional map, as originally done by Bailey et al. [25]. Moreover, the variational equation for determining the Lyapunov exponent (of the nonsmooth flow) is easily formulated and can be naturally computed alongside the numerical evolution of trajectories. Doing so has allowed us to give more detail to the Arnol'd tongue structure originally reported in [25]. Although chaos was not observed in this example, it is possible to find it in related models. In particular, one variant of the two-process model, first introduced in [44], has straight line trajectories between the upper and lower circadian processes, and when the lower circadian process is a constant function, as in the 'threshold' system of [24], we have found large regions of parameter space that support chaos using the method of Section 4. We have also highlighted the usefulness of saltation operators for treating the stability and bifurcation of (p, q) orbits in the two-process model, again circumventing the need for a map based approach. Other advantages of the nonsmooth perspective become more apparent when considering the use of the two-process model at the network level, and this is the main reason that we have developed the approach presented here.

Interestingly, at about the time that Borbély developed the two-process model, Petrillo and Glass developed a similar model for the synchronisation of respiration to a mechanical ventilator. This *two-factor* model also has activity that increases until it hits an upper periodically-modulated threshold and then decreases until it hits a lower periodically-modulated threshold [45]. Moreover, they show that nonsmooth two-factor models arise naturally in the study of the periodically forced van der Pol oscillator model (at least in some singular limit). The techniques developed here have equal applicability to these two-factor models and provide the applied mathematics community with another set of tools for their analysis.

Perhaps surprisingly, networks of sleepers and their collective dynamics have received very little attention in the mathematical biology community, although it is a topic of major interest in medicine and psychology, and see e.g. [26,46–48]. This is highly relevant to a society where a large number of adults share a bed with a partner. The potential implications for sleep quality, marital quality, and physical health are many and varied [43,47–49]. Indeed, the evidence that the individual sleeping behaviour of one partner influences the other's sleep is clear and perhaps unsurprising [46,49,50,50–53]. Therefore, exploring mathematical models of human sleep in the context of a dyad of co-habiting adults is an important topic, and one that can naturally build on the success of the two-process model albeit in a network setting. To do this one requires the specification of interaction between two sleepers. One natural way to do this would be to consider a direct state dependent interaction between sleepers or possibly an indirect state dependent modulation of the circadian process of one sleeper upon another. In either case the interaction would almost certainly be a continuous one during the time of bed sharing such that a network event based description would not be as general as one provided for by a network nonsmooth flow. In future work we will develop and analyse networks of interacting two process models using the nonsmooth approach developed here combined with tools from network science.

Declaration of competing interest

The authors declare that they have no known competing financial interests or personal relationships that could have appeared to influence the work reported in this paper.

Data availability

No data was used for the research described in the article.

Acknowledgements

This work was supported by the Engineering and Physical Sciences Research Council, UK [grant number EP/V04866X/1].

Appendix. Saltation operator

Here we derive the saltation rule at event time $t = T_1$ on the upper threshold. A similar calculation can be done at any event time $t = T_{2i+1}$ ($t = T_{2i}$), $i \in \mathbb{Z}$, on the upper (lower) threshold. We introduce indicator functions $h_1(x(t), t) = x(t) - H^+(t)$ and $h_2(x(t), t) = x(t) - H^-(t)$ such that switching events occur when $h_1(x(t), t) = 0$ and $h_2(x(t), t) = 0$ on the upper and lower threshold, respectively. Hence the unperturbed (perturbed) trajectory intersects with upper threshold at $t = T_1$ ($\tilde{T}_1 = T_1 + \delta T_1$) that is prescribed by $h_1(\bar{x}(T_1), T_1) = 0$ ($h_1(\tilde{x}(\tilde{T}_1), \tilde{T}_1) = 0$). Here we assume $\delta T_1 > 0$, however for the case $\delta T_1 < 0$ a similar argument holds. A Taylor expansion up to the first order terms yields

$$\begin{aligned} h_1(\tilde{x}(\tilde{T}_1), \tilde{T}_1) &= h_1(\tilde{x}(T_1 + \delta T_1), T_1 + \delta T_1) \\ &\simeq h_1(\tilde{x}(T_1) + \dot{\tilde{x}}(T_1)\delta T_1, T_1 + \delta T_1) \\ &\simeq h_1(\bar{x}(T_1) + \delta x(T_1) + \dot{\tilde{x}}(T_1^-)\delta T_1, T_1 + \delta T_1) \\ &\simeq h_1(\bar{x}(T_1), T_1) + \nabla_x h_1(\bar{x}(T_1), T_1)\left[\delta x(T_1) + \dot{\tilde{x}}(T_1^-)\delta T_1\right] \\ &\quad + \nabla_t h_1(\bar{x}(T_1), T_1)\delta T_1. \end{aligned} \tag{A.1}$$

Using this along with the property $h_1(\tilde{x}(\tilde{T}_1), \tilde{T}_1) = 0 = h_1(\bar{x}(T_1), T_1)$, we obtain

$$\nabla_x h_1(\bar{x}(T_1), T_1)\left[\delta x(T_1) + \dot{\tilde{x}}(T_1^-)\delta T_1\right] + \nabla_t h_1(\bar{x}(T_1), T_1)\delta T_1 = 0. \tag{A.2}$$

Moreover we have

$$\nabla_x h_1(x, t) = 1 \qquad \text{and} \qquad \nabla_t h_1(x, t) = -a^+\dot{C}(t). \tag{A.3}$$

Then by combining Eq. (A.2) and (A.3) we obtain

$$\delta x(T_1) + \dot{\tilde{x}}(T_1^-)\delta T_1 - a^+\dot{C}(t)\delta T_1 = 0. \tag{A.4}$$

Hence by solving Eq. (A.4) for δT_1 we find

$$\delta T_1 = -\frac{\delta x(t)}{\dot{\tilde{x}}(t) - a^+\dot{C}(t)}\bigg|_{t=T_1^-} = -\frac{\delta x(T_1^-)}{(1 - x(T_1^-))/\tau_w - a^+\dot{C}(T_1^-)}. \tag{A.5}$$

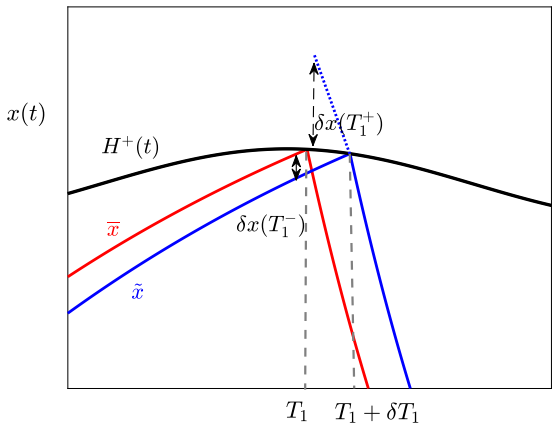

Fig. A.12. An illustration of the evolution of a perturbation at the upper switching threshold. The solid red line is the trajectory of an unperturbed orbit, with the event at time T_1. The solid blue line is the perturbed trajectory with an event at time $T_1+\delta T_1$ where $\delta T_1>0$. The approximation of $\tilde{x}(T_1^+)$ is given by the blue dotted line.

We can approximate $\tilde{x}(T_1^+)$ by pulling back the perturbed solution an amount of time δt starting from $\tilde{x}(\tilde{T}_1^+)$ and therefore we have that

$$\begin{aligned}\delta x(T_1^+) &\simeq \tilde{x}(T_1^+ + \delta T_1) - \dot{\tilde{x}}(T_1^+ + \delta T_1)\delta T_1 - \bar{x}(T_1^+)\\ &\simeq \bar{x}(T_1^+) + \delta x(T_1^-) + \dot{\tilde{x}}(T_1^-)\delta T_1 - \dot{\bar{x}}(T_1^+)\delta T_1 - \bar{x}(T_1^+)\\ &= \delta x(T_1^-) + \left[\dot{\tilde{x}}(T_1^-) - \dot{\bar{x}}(T_1^+)\right]\delta T_1\\ &= \delta x(T_1^-) + \left[\frac{1-x(T_1^-)}{\tau_w} + \frac{x(T_1^+)}{\tau_s}\right]\delta T_1,\end{aligned} \tag{A.6}$$

where we used the approximations $\dot{\tilde{x}}(T_1^-) = \dot{\tilde{x}}(T_1^-)$ and $\dot{\bar{x}}(T_1^+) = \dot{\tilde{x}}(\tilde{T}_1^+)$. An illustration of the evolution of a perturbation across the switching at time T_1 is given in Fig. A.12. We refer the interested reader to [32,35] that treats a similar situation for impacting systems. As a result, using Eq. (A.5) and (A.6) we obtain

$$\begin{aligned}\delta x(T_1^+) &= \left[1 - \frac{\left(\frac{1-\bar{x}(T_1^-)}{\tau_w}\right) - \left(-\frac{\bar{x}(T_1^+)}{\tau_s}\right)}{\frac{1-\bar{x}(T_1^-)}{\tau_w} - a^+\dot{C}(T_1^-)}\right]\delta x(T_1^-)\\ &\equiv K_1(T_1)\delta x(T_1^-),\end{aligned} \tag{A.7}$$

where $K_1(T_1)$ denotes the saltation rule and is given by

$$K_1(T_1) = \frac{a^+\dot{C}(T_1) + \frac{a^+}{\tau_s}C(T_1) + \frac{H_0^+}{\tau_s}}{a^+\dot{C}(T_1) + \frac{a^+}{\tau_w}C(T_1) + \frac{H_0^+-1}{\tau_w}}. \tag{A.8}$$

By following a similar method, the saltation rule $K_2(T_2)$ at $t=T_2$ on the lower threshold can be computed as

$$K_2(T_2) = \frac{a^-\dot{C}(T_2) + \frac{a^-}{\tau_w}C(T_2) + \frac{H_0^--1}{\tau_w}}{a^-\dot{C}(T_2) + \frac{a^-}{\tau_s}C(T_2) + \frac{H_0^-}{\tau_s}}. \tag{A.9}$$

We note that the saltation rule at any $t=T_{2i+1}$ on the upper threshold is prescribed by $K_1(T_{2i+1})$ and that of at any $t=T_{2i}$ on the lower threshold prescribed by $K_2(T_{2i})$.

References

[1] L. Besedovsky, T. Lange, J. Born, Sleep and immune function, Eur. J. Physiol. 463 (2012) 121–137.

[2] B. Rasch, J. Born, About sleep's role in memory, Physiol. Rev. 93 (2013) 681–766.

[3] C. Stroemel-Scheder, B. Kundermann, S. Lautenbacher, The effects of recovery sleep on pain perception: A systematic review, Neurosci. Biobehav. Rev. 113 (2020) 408–425.

[4] F.S. Luyster, P.J. Strollo, P.C. Zee, J.K. Walsh, Sleep: a health imperative, Sleep 35 (2012) 727–734.

[5] M.E. Thase, Depression and sleep: pathophysiology and treatment, Dialogues Clin. Neurosci. 8 (2006) 217–226.

[6] Z. Shan, H. Ma, M. Xie, P. Yan, Y. Guo, W. Bao, Y. Rong, C.L. Jackson, F.B. Hu, L. Liu, Sleep duration and risk of Type 2 diabetes: A meta-analysis of prospective studies, Diabetes Care 38 (2015) 529–537.

[7] J.-P. Chaput, C. Dutil, Lack of sleep as a contributor to obesity in adolescents: impacts on eating and activity behaviors, Int. J. Behav. Nutr. Phys. Activity 13 (2016) 1–9.

[8] F. Sofi, F. Cesari, A. Casini, C. Macchi, R. Abbate, G.F. Gensini, Insomnia and risk of cardiovascular disease: a meta-analysis, Eur. J. Prev. Cardiol. 21 (2014) 57–64.

[9] M.C. Moore-Ede, Mathematical Models of the Circadian Sleep-Wake Cycle, Tech. rep., Harvard Medical School Boston Ma, Dept of Physiology and Biophysics, 1984.

[10] R.E. Kronauer, C.A. Czeisler, S.F. Pilato, M.C. Moore-Ede, E.D. Weitzman, Mathematical model of the human circadian system with two interacting oscillators, Am. J. Physiol.-Regul. Integr. Comp. Physiol. 242 (1982) R3–R17.

[11] S. Daan, D.G. Beersma, A.A. Borbély, Timing of human sleep: recovery process gated by a circadian pacemaker, Am. J. Physiol.-Regul. Integr. Comp. Physiol. 246 (1984) R161–R183.

[12] S.H. Strogatz, Human sleep and circadian rhythms: a simple model based on two coupled oscillators, J. Math. Biol. 25 (1987) 327–347.

[13] R.W. McCarley, J.A. Hobson, Neuronal excitability modulation over the sleep cycle: a structural and mathematical model, Science 189 (1975) 58–60.

[14] R.W. McCarley, S.G. Massaquoi, A limit cycle mathematical model of the REM sleep oscillator system, Am. J. Physiol.-Regul. Integr. Comp. Physiol. 251 (1986) R1011–R1029.

[15] A. Phillips, P. Robinson, A quantitative model of sleep-wake dynamics based on the physiology of the brainstem ascending arousal system, J. Biol. Rhythms 22 (2007) 167–179.

[16] V. Booth, C.D. Behn, Physiologically-based modeling of sleep-wake regulatory networks, Math. Biosci. 250 (2014) 54–68.

[17] A.C. Skeldon, D.-J. Dijk, G. Derks, Mathematical models for sleep-wake dynamics: comparison of the two-process model and a mutual inhibition neuronal model, PLoS One 9 (2014) e103877.

[18] A.C. Skeldon, G. Derks, V. Booth, Nonsmooth maps and the fast-slow dynamics of sleep-wake regulation: Part II, in: Extended Abstracts Spring 2016, Springer, 2017, pp. 171–175.

[19] A.A. Borbély, S. Daan, A. Wirz-Justice, T. Deboer, The two-process model of sleep regulation: a reappraisal, J. Sleep Res. 25 (2016) 131–143.

[20] M. Nakao, M. Yamamoto, Bifurcation properties of the two process model, Psychiatry Clin. Neurosci. 52 (1998) 131–133.

[21] M. Nakao, H. Sakai, M. Yamamoto, An interpretation of the internal desynchronizations based on dynamics of the two-process model, Methods Inf. Med. 36 (1997) 282–285.

[22] M.R. Jeffrey, S. Webber, The hidden unstable orbits of maps with gaps, Proc. R. Soc. Lond. Ser. A Math. Phys. Eng. Sci. 476 (2020) 20190473.

[23] V. Avrutin, M.R. Jeffrey, Bifurcations of hidden orbits in discontinuous maps, Nonlinearity 34 (2021) 6140–6172.

[24] G. Derks, P.A. Glendinning, A.C. Skeldon, Creation of discontinuities in circle maps, Proc. R. Soc. Lond. Ser. A Math. Phys. Eng. Sci. 477 (2021) 20200872.

[25] M.P. Bailey, G. Derks, A.C. Skeldon, Circle maps with gaps: Understanding the dynamics of the two-process model for sleep–wake regulation, European J. Appl. Math. 29 (2018) 845–868.

[26] P.C. Rosenblatt, Two in a Bed: The Social System of Couple Bed Sharing, State University of New York Press, Albany, 2012.

[27] T. Deboer, Sleep homeostasis and the circadian clock: Do the circadian pacemaker and the sleep homeostat influence each other's functioning? Neurobiol. Sleep Circadian Rhythm. 5 (2018) 68–77.

[28] A.A. Borbély, A two process model of sleep regulation, Hum. Neurobiol. 1 (1982) 195–204.

[29] A.A. Borbély, P. Achermann, Sleep homeostasis and models of sleep regulation, J. Biol. Rhythms 14 (1999) 559–570.

[30] M.P. Bailey, Modelling sleep-wake regulation: the dynamics, bifurcations and applications of the two process model (Ph.D. thesis), University of Surrey, 2018.

[31] V.I. Arnold, Cardiac arrhythmias and circle mappings, Chaos 1 (1991) 20–24.

[32] M. di Bernardo, C. Budd, A.R. Champneys, P. Kowalczyk, Piecewise-Smooth Dynamical Systems: Theory and Applications, Vol. 163, Springer Science & Business Media, London, 2008.

[33] S. Coombes, R. Thul, Synchrony in networks of coupled non-smooth dynamical systems: Extending the master stability function, European J. Appl. Math. 27 (2016) 904–922.
[34] P.C. Müller, Calculation of Lyapunov exponents for dynamical systems with discontinuities, Chaos Solitons Fractals 5 (1995) 1671–1681.
[35] M.H. Fredriksson, A.B. Nordmark, On normal form calculations in impact oscillators, Proc. R. Soc. A 456 (2000) 315–329.
[36] S. Coombes, R. Thul, K.C.A. Wedgwood, Nonsmooth dynamics in spiking neuron models, Physica D 241 (2012) 2042–2057.
[37] R. Nicks, L. Chambon, S. Coombes, Clusters in nonsmooth oscillator networks, Phys. Rev. E 97 (2018) 032213.
[38] L. Dieci, R.D. Russell, E.S. Van Vleck, On the compuation of Lyapunov exponents for continuous dynamical systems, SIAM J. Numer. Anal. 34 (1997) 402–423.
[39] G. Benettin, L. Galgani, A. Giorgilli, J.-M. Strelcyn, Lyapunov characteristic exponents for smooth dynamical systems and for Hamiltonian systems; a method for computing all of them. Part 1: Theory, Meccanica 15 (1980) 9–20.
[40] M.T. Rosenstein, J.J. Collins, C.J. De Luca, A practical method for calculating largest Lyapunov exponents from small data sets, Physica D 65 (1993) 117–134.
[41] S.L.T. De Souza, I.L. Caldas, Calculation of Lyapunov exponents in systems with impacts, Chaos Solitons Fractals 19 (2004) 569–579.
[42] A.C. Skeldon, G. Derks, Nonsmooth maps and the fast-slow dynamics of sleep-wake regulation: Part I, in: A. Colombo, M. Jeffrey, J.T. Lázaro, J.M. Olm (Eds.), Extended Abstracts Spring 2016: Nonsmooth Dynamics, Vol. 8, Birkhäuser, 2017, pp. 167–170.
[43] K. Richter, S. Adam, L. Geiss, L. Peter, G. Niklewski, Two in a bed: The influence of couple sleeping and chronotypes on relationship and sleep. An overview, Chronobiol. Int. 33 (2016) 1464–1472.
[44] L. Glass, J. Belair, Continuation of Arnold tongues in mathematical models of periodically forced biological oscillations, in: H.G. Othmer (Ed.), Nonlinear Oscillations in Biology and Chemistry, in: Lecture Notes in Biomathematics, vol. 66, Springer-Verlag, Berlin, 1986, pp. 232–243.
[45] G. Petrillo, L. Glass, A theory for phase locking of respiration in cats to a mechanical ventilator, Am. J. Physiol.-Regul. Integr. Comp. Physiol. 246 (1984) R311–R320.
[46] W.M. Troxel, It's more than sex: Exploring the dyadic nature of sleep and implications for health, Psychosom. Med. 72 (2010) 578–586.
[47] R. Meadows, S. Arber, S. Venn, J. Hislop, N. Stanley, Exploring the interdependence of couples' rest-wake cycles: An actigraphic study, Chronobiol. Int. 26 (2009) 80–92.
[48] H.E. Gunn, D.J. Buysse, B.P. Hasler, A. Begley, W.M. Troxel, Sleep concordance in couples is associated with relationship characteristics, Sleep 38 (2015) 933–939.
[49] H.J. Drews, S. Wallot, S.L. Weinhold, P. Mitkidis, P.C. Baier, A. Roepstorff, R. Göder, "Are we in sync with each other?" Exploring the effects of cosleeping on heterosexual couples' sleep using simultaneous polysomnography: A pilot study, Sleep Disord. (2017) Article ID 8140672.
[50] H. Yoon, S.H. Choi, S.K. Kim, H.B. Kwon, S.M. Oh, J.-W. Choi, Y.J. Lee, D.-U. Jeong, K.S. Park, Human heart rhythms synchronize while co-sleeping, Front. Physiol. 10 (2019) Article 190.
[51] W.J. Strawbridge, S.J. Shema, R.E. Roberts, Impact of spouses' sleep problems on partners, Sleep 27 (2004) 527–531.
[52] M.B. Blumen, M.A.Q. Salva, I. Vaugier, K. Leroux, M.-P. d'Ortho, F. Barbot, F. Chabolle, F. Lofaso, Is snoring intensity responsible for the sleep partner's poor quality of sleep? Sleep Breath. 16 (2012) 903–907.
[53] F.P. Pankhurst, J. Home, The influence of bed partners on movement during sleep, Sleep 17 (1994) 308–315.